Journal of *Xenobiotics*

MDPI

Article

Closing the Loop: A Circular Approach to Sustainable Heavy Metal Remediation and Metal Recovery from Soil Leachates Using Tailor-Made Advanced Adsorbents

Paweł Miśkowiec [1,*], Alicja Katarzyńska [2], Dorota Majda [1], Xuan Tien Dao [1], Marcelina Radko-Zwierzyńska [1], Dariusz Cież [1] and Agnieszka Węgrzyn [1,*]

[1] Faculty of Chemistry, Jagiellonian University, Gronostajowa 2, 30-387 Kraków, Poland; dorota.majda@uj.edu.pl (D.M.); xuantien.dao@student.uj.edu.pl (X.T.D.); dariusz.ciez@uj.edu.pl (D.C.)
[2] Faculty of Chemical Engineering and Technology, Cracow University of Technology, Warszawska 24, 31-155 Kraków, Poland; alicja.katarzynska@doktorant.pk.edu.pl
* Correspondence: p.miskowiec@uj.edu.pl (P.M.); a.m.wegrzyn@uj.edu.pl (A.W.)

Abstract

This study investigates the remediation of natural soil samples from diverse locations, which exhibit varying degrees of copper contamination. To further elucidate the mechanisms of contaminant retention and desorption, similar extraction studies were conducted on representative soils. Finally, the resulting metal-rich leachates were treated using advanced organomodified adsorbents. This step aimed to reduce the volume of contaminated solutions and assess the potential for partial Cu recovery, thereby supporting a circular remediation concept.

Keywords: soil remediation; heavy metals; low molecular weight organic acids (LMWOA); functional mesoporous silica; metal recovery; circular economy

1. Introduction

The remediation of soils contaminated with heavy metals remains one of the most persistent environmental challenges worldwide [1–3]. Rapid industrialization, intensive agriculture, mining activities, and improper waste management have led to the accumulation of potentially toxic metals such as cadmium, lead, zinc, copper, and nickel in soils. Due to their non-biodegradable nature, long environmental persistence, and potential for bioaccumulation, heavy metals pose serious risks to ecosystems, food security, and human health [4,5]. Conventional remediation strategies often focus on immobilization or removal of contaminants, yet they frequently generate secondary waste streams and rarely address the long-term sustainability of the applied solutions [6].

In recent years, the concept of the circular economy has emerged as a key concept guiding the transformation of environmental management and resource use [7,8]. Unlike the traditional linear model based on extraction, consumption, and disposal, the circular economy emphasizes resource efficiency, waste minimization, and the recovery of valuable materials from secondary sources [9]. Within this framework, contaminated soils and remediation-derived effluents can be reconsidered not only as environmental liabilities but also as potential reservoirs of recoverable metals. Integrating remediation processes with metal recovery aligns soil protection goals with resource conservation and contributes to closing material loops.

Check for updates

Academic Editors: Liugen Zheng and Xing Chen

Received: 7 September 2026
Revised: 18 September 2026
Accepted: 30 October 2026
Published: 3 November 2026

Copyright: © 2026 by the authors. Licensee MDPI, Basel, Switzerland. This article is an open access article distributed under the terms and conditions of the Creative Commons Attribution (CC BY) license.

Beyond its general framing as a shift from a linear to a circular model, the circular economy places particular emphasis on recovering valuable metals from secondary resources. Contaminated soils and remediation-derived effluents may therefore be considered not only as environmental liabilities but also as potential sources of recoverable metals. The present study addresses a mixture of Cu, Cd, Pb, and Zn, which commonly co-occur in soils affected by mining and metallurgical activities. Cu is given particular attention because, among the metals investigated here, it exhibited the most pronounced selective and reversible binding behavior with the aminothiazole-functionalized sorbents, providing the clearest experimental basis for demonstrating metal recovery under the applied regeneration conditions. Moreover, copper is among the metals commonly identified as economically important due to its central role in electrification, renewable energy, and construction technologies, combined with finite primary reserves and supply-chain vulnerabilities [10–14]. Critical and rare metals, including rare-earth elements, are also increasingly relevant to circular-economy strategies [15,16]; however, their recovery is beyond the scope of the present study and represents a potential future application of the selective sorbent approach. Materials-chemistry approaches explicitly built around this agenda are increasingly common, from waste-derived catalysts designed for circular resource use to detailed mechanistic studies of how such sorbent/catalyst materials transform and regenerate over repeated use, which underpins their long-term reusability. Recovering metals from secondary sources, including mining- and smelting-impacted soils and their remediation effluents, is therefore increasingly viewed not only as an environmental obligation but as a genuine resource-recovery opportunity, sometimes described as “urban” or “anthropogenic” mining. This philosophy extends naturally to the adsorbents themselves. Industrial by-products such as aluminum saline slag have been valorized as raw materials for functional clay-based materials, and the waste liquor generated during acid activation of vermiculite has been converted into layered-double-hydroxide hybrid adsorbents active toward Cu^{2+} and dyes [17], with a wet fine-milling pre-treatment step before acid activation further improving the efficiency of this preparation route. Such waste-derived, low-cost adsorbents have repeatedly proven capable of handling diverse pollutant classes, from pharmaceuticals to the simultaneous removal of dyes and metal cations by the same sustainable, recyclable material [18], to dual-function sorbents that combine pollutant capture with additional storage functionality, underscoring that a single tailor-made material can plausibly address more than one contaminant at once. Viewed this way, soils historically contaminated by industrial or mining activity can be regarded as diffuse, low-grade secondary deposits. Although metal concentrations are far below those of primary ores, the scale of contaminated land, the mounting heavy-metal pressure this places on soil and water ecosystems, and the regulatory pressure to remediate it make selective, low-cost recovery strategies both economically and environmentally attractive. Embedding metal recovery directly into the remediation workflow, rather than treating it as an afterthought, is therefore a concrete way to align soil protection with the broader secondary raw materials agenda.

Soil washing and leaching techniques are widely applied for the removal of heavy metals from contaminated soils, particularly in cases where metals occur in mobile or weakly bound fractions. These approaches, often assisted by chelating agents or environmentally benign extractants, can effectively transfer metals from the solid phase into aqueous leachates [19–21]. However, the resulting metal-rich solutions require further treatment to prevent secondary pollution and to enable safe disposal or reuse. From a circular perspective, this step represents a critical opportunity for selective metal capture and recovery rather than simple neutralization or dilution. Advanced adsorbent materials have attracted increasing attention as efficient tools for the treatment of metal-containing aqueous streams. Tailor-made adsorbents, designed with specific surface functionalities,

porosity, and selectivity, offer the possibility of targeting individual metal ions even in complex matrices [22–24]. Compared to conventional sorbents, such materials can combine high adsorption capacity with regeneration potential, thereby supporting repeated use and reducing overall material consumption. When applied to soil leachates, advanced adsorbents can simultaneously contribute to environmental risk reduction and the recovery of metals for potential reuse in industrial or technological applications.

The present study explores this opportunity by proposing and testing a closed-loop treatment scheme, illustrated in Figure 1, in which contaminated soil is first washed with a mild, environmentally benign leaching agent, and the resulting metal-laden washing effluent is then treated with tailor-made adsorbents to selectively capture the leached metals. By recovering the metals from the effluent and enabling regeneration of both the sorbent and the aqueous phase, this approach aims to close the water loop of the soil-washing process, reducing the volume and toxicity of the waste stream that ultimately requires disposal while simultaneously generating a metal-rich, recoverable output stream.



Figure 1. Proposed closed-loop water management scheme for heavy-metal-contaminated soil remediation.

The aim of this work is as follows.

- To analyze the efficiency of copper leaching from exemplar contaminated soils and model systems using environmentally friendly reagents, with acetic acid as the primary example.
- To investigate the potential recovery of copper from the resulting leachates, in line with circular-economy principles of secondary raw material recovery.
- To design and characterize tailor-made organomodified SBA-15 adsorbents, obtained by post-synthesis grafting and by co-condensation and functionalized with aminothiazole and aminobenzothiazole groups, for the capture of heavy metals from soil leachates.
- To evaluate the adsorption capacity and metal selectivity of these adsorbents in both single-metal and competitive multi-metal aqueous model systems selected on the basis of metal compositions observed in the soil-washing leachates.
- To assess the reusability of the best-performing adsorbents through repeated adsorption/desorption cycles, thereby evaluating the potential for metal recovery and treated-water reuse within the proposed closed-loop scheme.

2. Materials and Methods

2.1. Chemicals

All reagents employed in the experiments were of high-purity analytical grade, and no additional purification was performed prior to use. Deionized (DI) water was used to prepare all preparation steps. Standard solutions of Pb, Zn, Cu, and Cd were used to calibrate the analytical instrument. Sample digestion was employed using 65% HNO_3 (POCH, Gliwice, Poland) and 30% H_2O_2 (Chempur, Piekary Śląskie, Poland).

Citric acid (Thermo Scientific, Waltham, MA, USA) and acetic acid (Chempur, Piekary Śląskie, Poland) were used as biochelators for the soil washing test. High-purity acetylene and argon gas were supplied for flame atomic absorption spectrometry (F-AAS). In adsorption experiments, chloride or acetate metal salts were used: $ZnCl_2$, $CdCl_2 \cdot 2.5H_2O$, $CuCl_2 \cdot 2H_2O$, $Pb(CH_3COO)_2 \cdot 3H_2O$, $Cd(CH_3COO)_2 \cdot 2H_2O$, $Cu(CH_3COO)_2 \cdot H_2O$ (Warchem, per analysis, Zakręt, Poland).

2.2. Soil Sample Collection

Samples were collected along a gradient of metal concentration, from relatively low to high, in the vicinity of the Bukowno mine and smelter, located within the major local source area of heavy-metal contamination in the region [25–27]. The concentrations of the selected elements (Cd, Zn, Pb, and Cu) as a function of distance from the potential source of contamination are presented in Figure 2.

The investigated area forms part of the Olkusz–Bukowno Zn–Pb ore-bearing region, which has been affected by long-term mining, ore processing, and metallurgical activities. The contamination is therefore considered a chronic and cumulative anthropogenic impact rather than the result of a single pollution event. Historically, metals were introduced into the environment through mining and metallurgical wastes, atmospheric deposition associated with ore processing and smelting, and dust dispersion from tailings and waste-storage areas. Long-range atmospheric transport from the Upper Silesian industrial region has also contributed to the regional contamination [25–28]. Mining in the Olkusz–Bolesław region has been documented since at least the twelfth century, while industrial-scale exploitation and metallurgical activity intensified during the nineteenth and twentieth centuries. In the post-war period, the industrial complex in Bukowno was substantially developed, with zinc-processing and metallurgical facilities becoming operational during the 1950s.

The soils of the Olkusz–Bukowno region are heterogeneous. In the immediate ore-bearing area, rendzina-type soils predominate, while sandy/eolian deposits and other soil types also occur [26].

The samples were obtained exclusively from non-forested sites, including arable fields and grasslands, in order to eliminate the influence of tree cover on the results. Soil was collected from the surface down to a depth of 0.3 m, corresponding to the topsoil horizon. The selected 0–0.30 m layer was intended to provide a representative sample of the contaminated topsoil for the subsequent soil-washing experiments, while limiting the contribution of deeper parent material and potentially geogenic metal concentrations. This sampling depth is also consistent with the approach used in previous investigations of heavy-metal contamination in the Olkusz District and with the 0–0.30 m topsoil interval used in regional soil-quality and geochemical assessments [29]. The use of a standardized topsoil interval also provides comparability with previous studies conducted in the region [25]. At every sampling point, a minimum of 10 subsamples were gathered within an area of about 10 × 10 m and combined into a single composite sample with a mass of up to 1 kg. The collected material was then air-dried, crushed, and passed through a 2 mm sieve. Afterward, each initial sample was quartered into four equal parts. Three portions were rejected, while the remaining one, treated as the laboratory sample, was retained for further analyses.

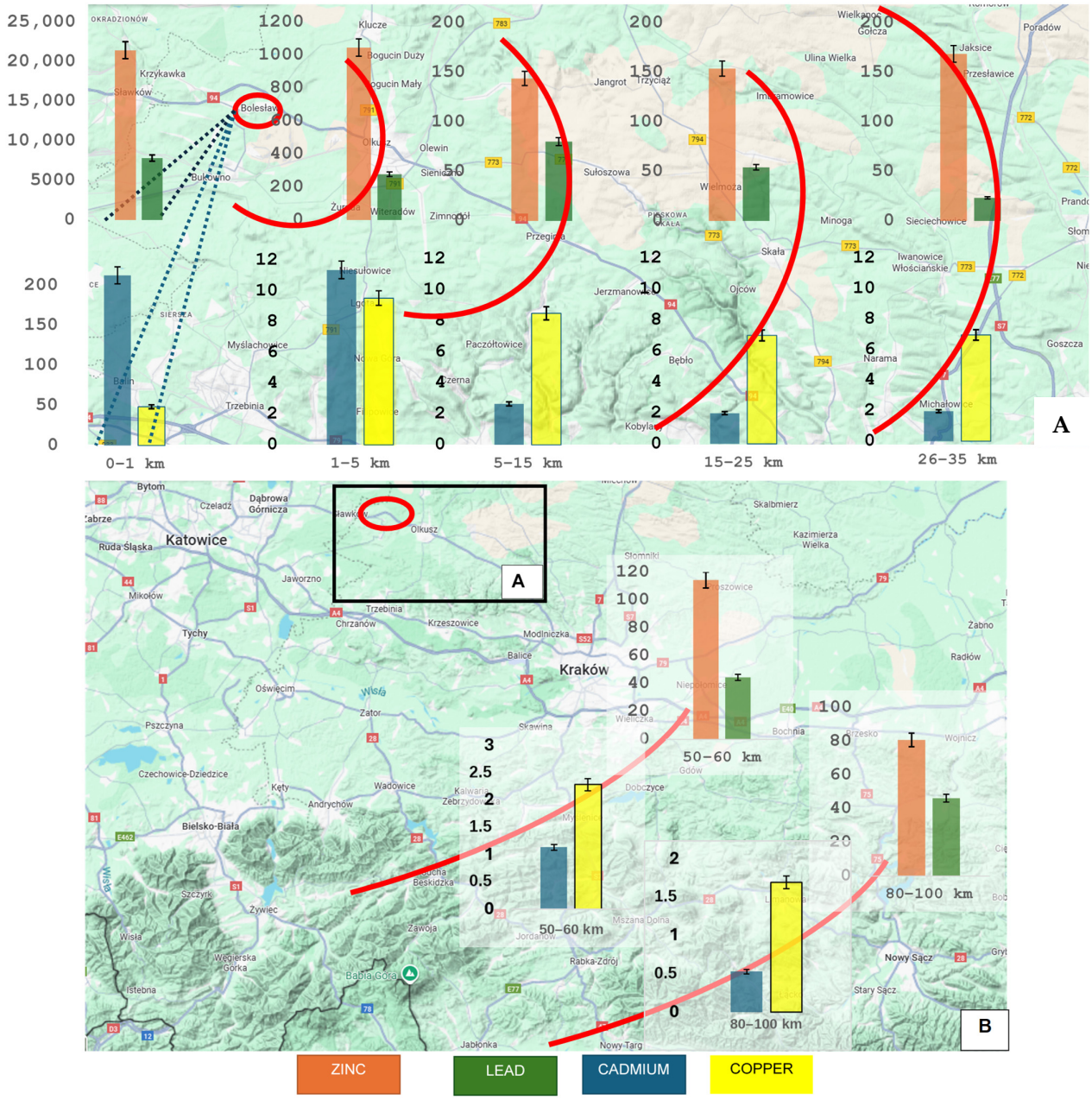

Figure 2. Soil concentrations of cadmium (Cd), zinc (Zn), copper (Cu), and lead (Pb) in mg/kg of dry mass of soil, as a function of distance from the potential emission source (Bukowno zinc smelter). Up to 35 km (**A**) and 50–100 km (**B**). Red arcs indicate approximate distance boundaries (in km) from the smelter; red ellipses mark its location.

To characterize the soils, basic physicochemical properties were determined, namely pH, clay fraction proportion, and organic matter content. A detailed description of the analytical procedures has been provided in our earlier publications [25]. Soil pH was measured potentiometrically in 1.0 M KCl solution in accordance with ISO 10390:2005, using an Elmetron CP-461 pH meter [30]. The clay fraction percentage was established by the Bouyoucos hydrometer method as modified by Casagrande and Proszynski [31]. Organic carbon content was determined with the Shimadzu SSM-5000A carbon analyzer (Shimadzu Corporation, Kyoto, Japan), and the results were expressed as percentage values.

2.3. Mineralization of the Original Soil Samples

For the digestion procedure, 1.5 g of soil was accurately weighed to the nearest 0.0001 g using an analytical balance and transferred into a Teflon vessel (ERTEC-POLAND, Wrocław, Poland). Subsequently, 4 mL of hydrogen peroxide and 10 mL of concentrated nitric acid were added. Once the initial vigorous oxidation reaction had ceased and foaming was no longer observed, the samples were mineralized using the Ertec Magnum II digestion system (ERTEC-POLAND, Wrocław, Poland). After completion of the process, the obtained solution was filtered into a 25 mL volumetric flask. The applied procedure was consistent with the US EPA standard and corresponded with the methodologies used in our previous studies [32,33].

2.4. Extraction Analysis of Soil Samples

Acetic acid was selected as an example of an inexpensive and widely available low-molecular-weight organic acid (LMWOA) for the leaching of metals from soils with varying contamination levels. Citric acid, in turn, was used as a reference compound, as it is one of the most commonly applied LMWOAs in soil remediation processes [34].

Two series of soil-washing experiments were carried out. In the first series, 0.01 M acetic acid was applied, whereas in the second, 0.01 M citric acid was used for comparison. The soil-to-solution ratio was maintained at 1:10, corresponding to 2.0 g of soil mixed with 20.0 mL of acid solution. The suspensions were subjected to mechanical shaking for contact times of 15 min, 1 h, and 4 h. After extraction, the samples were centrifuged at 6000 rpm, and the supernatants were decanted and subsequently filtered.

All filtered extracts were analyzed by flame atomic absorption spectrometry (F-AAS) using a Contraa 800 atomic spectrometer (Analytik Jena, Jena, Germany). Copper, cadmium, zinc, and lead were selected as target analytes in order to assess both the efficiency of their removal from soil and the subsequent effectiveness of metal recovery from the obtained solutions.

The limits of detection (LOD) were calculated as three times the standard deviation of repeated blank solution measurements. The obtained values were 4 $\mu g/dm^3$ for copper, 5 $\mu g/dm^3$ for zinc, 7 $\mu g/dm^3$ for lead, and 1.5 $\mu g/dm^3$ for cadmium.

2.5. Synthesis of the Organic Ligands and Their Incorporation into SBA-15

Tailor-made organic ligands designed to capture cationic pollutants (metals) were synthesized by reacting (3-chloropropyl)-trimethoxysilane or (3-isocyanatopropyl)-triethoxysilane with the target heterocyclic amines, 2-aminothiazole and 2-aminobenzothiazole [35]. The resulting organosilanes were incorporated into ordered hexagonal mesoporous silica (SBA-15) by two independent routes: (i) homogeneous post-synthesis grafting onto a pre-formed SBA-15 support, and (ii) co-condensation of the organosilane with the silica precursor during SBA-15 synthesis (sample codes prefixed X). For the grafted materials, two different parent SBA-15 batches were used, denoted by the prefixes A and B, depending on parent silica pore size. Details of synthesis and physicochemical characterization of precursors are presented in Supplementary Materials Chapter S1. The molecular structures and abbreviations of the synthesized anchoring compounds are summarized in Table S1, while detailed synthesis procedures for the modified organosilanes, co-condensation, and post-synthesis grafting are provided in Section S1. The five adsorbents used in the adsorption study are therefore AAmBenS and BAmS (grafted, on pore-size-matched parent silicas), and XAmBenS and XAmS (co-condensed). Successful incorporation of both ligands by both routes, and the associated decrease in pore size and pore volume upon grafting without loss of the underlying hexagonal pore ordering, were confirmed by physicochemical characterization.

Detailed spectroscopic evidence for the successful formation of the anchoring compounds is provided in the Supplementary Material (Section S2.1, Figures S1–S3 and Tables S2 and S3).

2.6. Purification of the Co-Condensed Adsorbents

The co-condensed adsorbents (XAmS, XAmBenS) were purified by Soxhlet extraction before use to remove the structure-directing agent (Pluronic P123) and any unreacted organosilane. Approximately 1 g of ground XAmS, or 1.3 g of ground XAmBenS, was placed in a paper extraction thimble and extracted in two consecutive stages: first with a methanol/acetic acid mixture (90:10, *v*/*v*, 117 mL methanol + 13 mL acetic acid), and subsequently with pure methanol (130 mL), each stage lasting approximately 10–12 h under reflux. Small portions of the purified solid and of the spent solvent were withdrawn after each stage (stage I at half-time, and stage II, which was equivalent to the finished process) and analyzed by infrared (IR) spectroscopy and X-ray diffraction, together with reference spectra of P123, methanol, acetic acid, and the methanol/acetic acid mixture, to confirm removal of the template. The corresponding FT-IR and XRD monitoring data are provided in Figures S5 and S7 of the Supplementary Material. The extraction was repeated for a fresh batch of samples with methanol only (140 mL, Soxhlet). Two purification batches of XAmS were thereby obtained, and both were carried forward into the adsorption experiments: XAmS(MA), extracted with the methanol/acetic acid mixture, and XAmS(M), extracted with methanol only. XAmBenS was purified with methanol only (XAmBenS(M)).

2.7. Metal Adsorption and Regeneration in Liquid Systems

Adsorption properties of synthesized organo-modified silica adsorbents were determined in a single-metal solution (Cu) as well as multicomponent mixtures.

2.7.1. Cu Adsorption from a Single-Component Solution

The adsorption experiments were carried out in polypropylene vessels by adding 25 mg of the functionalized SBA-15 to 10 mL of 1 mmol L^{-1} (63.5 mg Cu^{2+} L^{-1}) copper solution in the form of chloride or acetate. The resulting mixture was stirred at 25 °C for 2.5 h.

2.7.2. Batch Adsorption Screening (Single-Run Experiments) in Multi-Metal Aqueous Solutions

Batch adsorption tests were carried out using synthetic multi-metal aqueous solutions prepared from analytical-grade metal salts: $Pb(CH_3COO)_2{\cdot}3H_2O$, $Cd(CH_3COO)_2{\cdot}2H_2O$ and $Cu(CH_3COO)_2{\cdot}H_2O$ for the acetate-based ternary system (Pb–Cd–Cu, "PCC"), and $CdCl_2{\cdot}2.5H_2O$, $ZnCl_2$ and $CuCl_2{\cdot}2H_2O$ for the chloride-based ternary system (Zn–Cd–Cu, "ZCC"). The metal combinations selected for these model systems were based on the composition of the soil-washing leachates obtained in the preceding experiments. The synthetic solutions were not intended to reproduce the complete chemical composition of the authentic leachates, but to provide controlled model systems for studying competitive metal adsorption and regeneration. Individual 100 mL stock solutions of each salt were prepared at a nominal concentration of 1.5 mmol/L. For each adsorption test, 10 mg of adsorbent was contacted with 3 mL of each of the three relevant metal-salt stock solutions (9 mL total per test; solid/liquid ratio close to 1.1 g/L), giving a nominal concentration of 0.5 mmol/L per metal in the resulting solution. A second series of experiments extended the ZCC system to a five-fold higher Zn loading (2.5 mmol/L Zn, Cd and Cu unchanged at 0.5 mmol/L) to probe the sorbents' response to a higher competing-metal load. Two blank solutions (50 mL of 0.1 mmol/L HCl and 50 mL of 0.1 mmol/L acetic acid) were run alongside the metal solutions as background controls. Suspensions were agitated by shaking for 18 h at room temperature, after which they were centrifuged and the supernatants

diluted ten-fold prior to determination of residual metal concentration by flame atomic absorption spectroscopy (AAS) and evaluated by ion chromatography (IC) for the ZCC system. Each sorbent/metal-mixture combination was run in triplicate. The initial screening set comprised the three aminothiazole-based sorbents (XAmS(M), XAmS(MA), BAmS); an analogous screening of the aminobenzothiazole-based sorbents (AAmBenS, XAmBenS(M)) was carried out following the same protocol. Cu uptake after the 18 h contact period (apparent equilibrium uptake) (q_e, in mg/g and mmol/g) and removal efficiency (R, %) were calculated from the difference between initial and residual metal concentration, according to the following equations:

q_e (mg/g)—adsorption amount of copper:

$$q_e = \frac{V \times (C_0 - C_e)}{m} \quad (1)$$

R_{ads} (%)—adsorption efficiency:

$$R_{ads} = \left(1 - \frac{C_e}{C_0}\right) \times 100\% \quad (2)$$

where

V (dm^3)—volume of copper solution;
C_0 (mg/dm^3)—initial adsorbate concentration;
C_e (mg/dm^3)—adsorbate concentration after the 18 h contact period;
m (mg)—mass of the adsorbent.

q_e values were also expressed as mmol/g; therefore, it was possible to calculate the percentage of functional groups involved in the adsorption process (occupied functional groups [%]).

2.7.3. Adsorption–Desorption Cycling Experiments in Multi-Metal Aqueous Solutions

To assess sorbent reusability, the two best-performing co-condensed adsorbents from the screening step, XAmS(M) and XAmBenS(M), were subjected to five consecutive adsorption/desorption cycles in both the PCC and ZCC ternary systems (0.5 mmol/L per metal). Each adsorption step used the same solid/liquid conditions as the single-run screening (10 mg adsorbent contacted with 3 mL of each of the three metal-salt stock solutions, 9 mL total, 0.5 mmol/L per metal) and the same 18 h contact time, but unlike the screening experiments, each cycle was run once, without triplicate repetition, to limit the sample usage and analysis burden of the multi-cycle protocol. After each adsorption step, the loaded sorbent was separated, the supernatant analyzed by AAS, and the sorbent then subjected to a desorption (regeneration) step with 9 mL of 0.01 M HCl solution followed by a wash step before being returned to a fresh aliquot of metal solution for the next adsorption cycle. This adsorption/desorption/wash sequence was repeated for five cycles per sorbent/matrix combination. From the resulting concentration data, per-cycle and cumulative metal uptake (Q_{ads}, $Q_{cum,ads}$), per-cycle and cumulative metal recovered (Q_{des}, $Q_{cum,ads}$), capacity retention (CR, %, relative to cycle 1) and desorption efficiency (DE, %, fraction of the adsorbed metal recovered in the corresponding desorption step) were calculated. Definitions and calculation procedures for Q_{ads}, Q_{des}, capacity retention, desorption efficiency, and cumulative recovery are provided in Supplementary Material, Section S3.

2.8. Instrumental Methods for Sample Analysis

Copper, cadmium, zinc, and lead have been chosen to check both the efficiency of leaching from the soil using LMWOA and the efficiency of metal adsorption from liquid solutions via adsorption.

The solutions obtained from the soil samples digestion and adsorption experiments were analyzed to determine the contents of particular metals with flame atomic absorption spectrometry (F-AAS), using the contrAA 800 model (Analytik Jena, Jena, Germany). Based on the results of three independent measurements performed for each sample, the average values of copper, cadmium, lead, and zinc concentrations as well as the relative standard deviations were calculated. The detection limits were determined as a 3-fold standard deviation of repeated measurements of a blank solution and were 4 $\mu g/dm^3$ for copper, 5 $\mu g/dm^3$ for zinc, 7 $\mu g/dm^3$ for lead, and 1.5 $\mu g/dm^3$ for cadmium.

For single-metal Cu-containing liquid samples, after metal recovery from liquid solutions via adsorption, metal determination was performed using Ion Chromatography (IC) HIC-ESP LC-20Ai (Shimadzu, Kyoto, Japan). Analysis conditions were as follows: column Shim-pack IC-C4 (150 mm/L × 4.6 mm I.D., 7 µm), mobile phase A) 2.5 mmol/L oxalic acid and B) 2.5 mmol/L methanesulfonic acid, A/B = 60/40 (*v*/*v*), flow rate 1.0 mL/min, column temperature 40 °C, detector CDD-10A VP, injection volume 20 µL.

The percentage content of hydrogen, carbon, nitrogen, and sulfur in organo-modified silica adsorbents (CHNS) was determined using a Vario Micro Cube elemental analyzer with electronic microbalance (Elementar Analysensysteme GmbH, Langenselbold, Germany).

Infrared spectra of the samples were recorded using the attenuated total reflectance technique with a Nicolet iS5 FTIR (Thermo Scientific, Madison, WI, USA) equipped with an iD3 ATR module with a germanium crystal window. The number of scans recorded during a single spectral measurement was 64, with a resolution of 2 cm^{-1}. Absorbance spectra were recorded in the 4000–525 cm^{-1} range.

The ^1H NMR spectra were recorded using a Bruker Avance II 300 MHz spectrometer (Bruker BioSpin, Fällanden, Switzerland) with TMS as an internal standard.

The structure of the materials was characterized by an X-ray powder diffractometer BRUKER D2 PHASER (Bruker AXS, Karlsruhe, Germany) equipped with a CuKα radiation source. The patterns were collected in the 2θ range of 0.5° to 4° with a step of 0.02°.

UV–vis spectra of Cu-containing solutions were recorded on an Evolution 220 (Thermo Scientific, Madison, WI, USA) spectrophotometer in the range of 190–900 nm with a resolution of 2 nm.

UV–vis-DRS spectra of organo-modified silica adsorbents before and after adsorption were recorded on an Evolution 600 (Thermo Scientific, Madison, WI, USA) spectrophotometer in the range of 190–900 nm with a resolution of 4 nm.

Thermoporometry (TPM) investigations were performed using a Mettler Toledo apparatus DSC 822^e (Mettler Toledo, Greifensee, Switzerland), with an accuracy of 4 10^{-6} W, equipped with a liquid nitrogen cooling system (Criofab, Kenilworth, NJ, USA) allowing work between −140 and 400 °C. Apparatus calibration for heat flux and temperature was performed with n-octane, indium, and zinc standards provided by the supplier. The tolerance in the instrument calibration is 0.2 °C. Before the TPM experiment, a sample was placed in an aluminum pan, water was added, and the pan was sealed with a lid. To avoid the supercooling effect, the samples were quenched far below the equilibrium freezing temperature (to −30 °C) with the cooling rate β = 10 K/min and then heated with β = 2 K/min to +10 °C [36]. After the experiment, a small hole was made in the lid of the crucible, and the sample was heated up to 200 °C in order to evaporate the liquid component and obtain the sample mass. Pore size distribution was determined from the solid-to-liquid DSC profiles. For the structural calculations reported in Section 3.2, the pore dimension used in the wall-thickness estimate was taken from the corresponding BJH or thermoporometric pore-size determination, as indicated in the table footnote. Because the XRD and thermoporometric measurements may refer to samples with different hydration or thermal histories, the resulting wall-thickness values are considered approximate structural

estimates. The melting point depression was obtained relative to the excess phase, so that each experiment was internally calibrated for temperature [37].

3. Results and Discussion

3.1. Soil Decontamination

The efficiency of metal leaching from the selected soil samples with acetic acid, and in comparison with citric acid, is depicted in Figure 3.

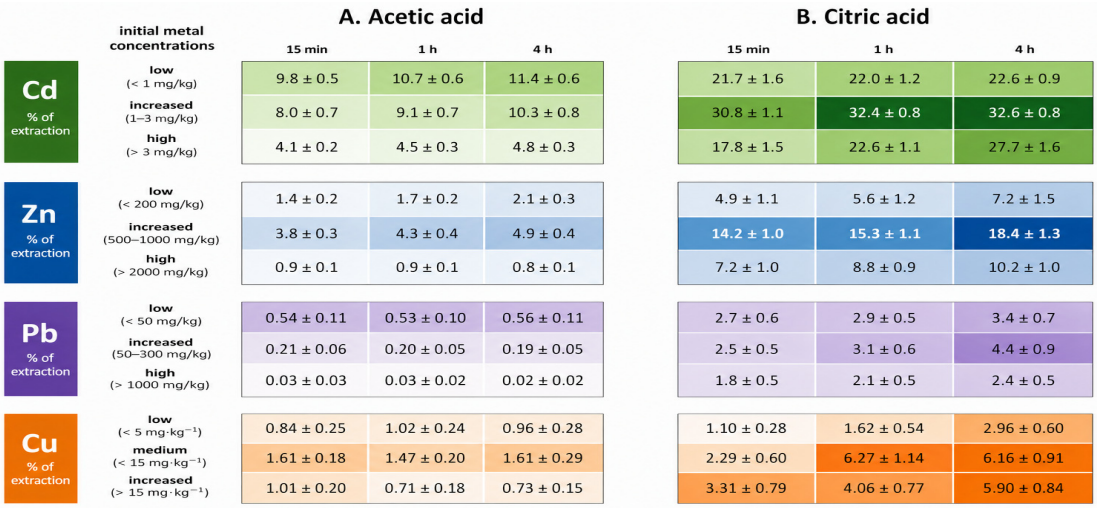

Figure 3. Heatmap visualization of the extraction efficiency of Cd, Zn, Pb, and Cu with acetic (**A**) and citric acids (**B**), expressed as the percentage of the total metal content released after 15 min, 1 h, and 4 h of washing. Values shown in each cell represent the mean extraction percentage ± uncertainty. Color intensity increases with extraction efficiency within each metal, enabling direct comparison between acids and extraction times. Soil samples were classified into three groups according to their initial metal concentrations: low, increased, and high for Cd, Pb, and Zn, and low, medium, and increased for Cu, reflecting natural variability in soil contamination.

Figure 3 illustrates that although acetic acid is notably less effective than citric acid, its performance provides essential insights for evaluating the feasibility of mild-organic-acid soil washing systems, especially where low cost, low environmental burden, and on-site applicability are priorities.

Acetic acid extracted up to 10–11% of total Cd within 4 h in soils with low and increased contamination, and typically 4–5% in highly contaminated soils. This moderate efficiency, though significantly lower than citric acid, indicates that acetic acid is capable of mobilizing a meaningful fraction of Cd even without strong complexation. Zn showed the highest extraction efficiency with acetic acid, reaching 4–5% after 4 h. This reflects Zn's relatively weaker binding in many soil matrices. Despite still being lower than the citric acid counterpart, the values confirm that acetic acid is able to remove a non-negligible portion of Zn even in more contaminated soils. Pb extraction with acetic acid remained consistently low (≤0.6%), irrespective of soil contamination class or duration of washing. This confirms the strong association of Pb with mineral phases and its limited susceptibility to weak organic acids. The contrast with citric acid (up to ~5%) highlights the limitations of mild organic acids in addressing strongly sorbing contaminants such as Pb. However, it also emphasizes that Pb remains largely immobilized in the soil even after washing, reducing risks of secondary spreading. Acetic acid extracted ~0.9–1.6% of total Cu, placing this metal between Zn and Pb in terms of susceptibility to mild-organic-acid mobilization. The limited extraction reflects Cu's tendency to form stable complexes with soil organic matter and mineral surfaces, which acetic and citric acids only partially disrupt. From a

remediation perspective, these results indicate that 0.01 M acetic acid provides only limited removal of strongly retained metals, particularly Pb and Cu. Thus, the present washing conditions should be regarded as a mild mobilization treatment rather than a stand-alone approach for extensive soil decontamination. Their main advantage is the generation of a comparatively mild washing effluent while avoiding excessively aggressive extraction conditions. Further optimization would be required where greater removal of strongly retained metals is targeted.

Even though acetic acid shows modest extraction percentages (Figure 3), the absolute concentrations of metals measured in the washing solutions (Table 1) reveal that even this mild organic acid generates effluents that cannot be discharged without treatment.

Table 1. Concentration ranges of selected heavy metals in leachates obtained after soil washing with acetic and citric acids.

Metal	Concentration Range in Acetic Acid Leachates (mg/L)	Concentration Range in Citric Acid Leachates (mg/L)
Cadmium (Cd)	0.005–0.27	0.01–1.7
Lead (Pb)	0.013–0.20	0.06–12.1
Zinc (Zn)	0.11–32	0.21–234
Copper (Cu)	0.004–0.02	0.03–0.10

Table 1 clearly demonstrates that, for instance, Cd concentrations in acetic acid leachates may reach 0.27 mg/L (depending on soil class), which already exceeds commonly accepted limits for direct discharge to surface waters or sewer systems due to the high toxicity of this element [38]. In soils with increased contamination, Cd concentrations in leachates approach or surpass values classified as "requiring purification" under many environmental guidelines [39,40]. In the case of lead, despite the extraction never exceeding 0.6% with acetic acid and 4.5% with citric acid, the concentration in leachates still reaches 0.2 mg/L in acetic acid leachates from soils with high initial Pb content, and exceeds 12 mg/L in the case of citric acid leaching. This occurs because even a very small extraction fraction corresponds to a sizeable absolute mass transfer at elevated soil Pb levels. These values also exceed the maximum allowable concentration of this element in surface water and must be subjected to a purification process [40]. Moreover, other studies confirmed the toxic impact of those metals on living organisms and human health even at low concentrations [41,42].

Zn concentrations in acetic acid effluents, however, are generally lower than in citric acid filtrates, but still reach as much as 32 mg/L for leachates from soils with increased or high Zn content. In the case of citric acid, this value is over 7 times higher. Although Zn is less critical from a toxicological standpoint, these values may exceed standard reuse or irrigation limits [43]. Copper, forming relatively stable soil complexes, appears in acetic acid filtrates at moderate levels (up to 0.02 mg/L with acetic acid and 0.1 mg/L with citric acid), yet these may still surpass allowed concentrations for direct environmental release [44].

The ranges reported in Table 1 underscore a crucial point: even when a weak acid such as acetic acid is used, the resulting leachates frequently contain metal concentrations high enough to require dedicated purification.

3.2. Adsorbent Properties

Structural parameters of the SBA-15 synthesized under different conditions (synthesis A and B) and of the grafted samples are presented in Table 2. The low-angle XRD diffractograms recorded for the synthesized samples are presented in Figures 4–6.

Table 2. Calculation of structural parameters for SBA-15 prepared by synthesis A, B, post-synthesis grafting with functional groups, co-condensation, and samples after adsorption.

Sample Name	2θ [°]	d_{100} [nm]	a_0 [nm]	W or W^{TPM} [nm]
A	0.984	8.97	10.4	5.2
B	0.920	9.59	11.1	4.9
BAmS *	0.933	9.46	10.9	* 5.3/4.7 $^{TPM\ non\text{-}calc}$ vs. 3.7 $^{TPM\ calc}$
XAmS	0.850	10.38	12.0	-
XAmS M stage I	0.895	9.86	11.4	-
XAmS M stage II	0.926	9.53	11.0	-
XAmS MA stage I	0.872	10.12	11.7	-
XAmS MA stage II	0.907	9.73	11.2	-
XAmS M PCC	0.860	10.26	11.9	-
XAmS M ZCC	0.882	10.00	11.6	-
XAmS MA PCC	0.855	10.32	11.9	-
XAmS MA ZCC	0.909	9.71	11.2	-
AAmBenS *	0.998	8.85	10.2	* 5.3/5.4 $^{TPM\ non\text{-}calc}$ vs. 3.9 $^{TPM\ calc}$
XAmBenS	0.820	10.77	12.4	-
XAmBenS M stage I	0.852	10.37	12.0	-
XAmBenS M stage II	0.854	10.34	11.9	-
XAmBenS M PCC	0.831	10.63	12.3	-

where d_{100} is the XRD (100) interplanar spacing; a_0 is the unit cell parameter ($a_0 = 2 \times (d_{100}/\sqrt{3})$; W is the estimated pore-wall thickness ($a_0 - D_{BJH}$); D_{BJH} is the BJH pore diameter; *—porosity measured after calcination; ^{TPM}—pore size for calculations was adopted from thermoporometry of non-calcined or calcined samples.

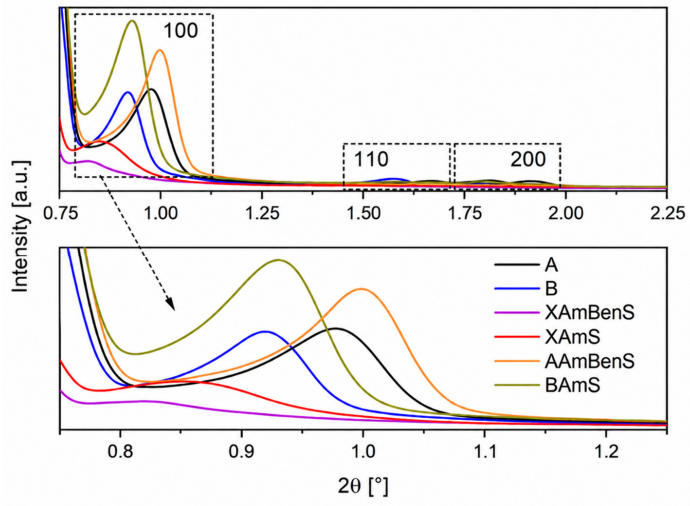

Figure 4. XRD patterns of as-prepared SBA-15 adsorbents with organic functional groups.

The presence of the characteristic diffraction peaks (100), (110), and (200) proves that the obtained materials have a highly ordered porous structure [45]. The successful formation of the corresponding anchoring compounds was independently confirmed by FT-IR and ^1H NMR spectroscopy (Supplementary Material, Figures S1–S3; Tables S2 and S3). The observed vibrational bands are consistent with previously reported spectroscopic

data for the corresponding organosilane and heterocyclic structures [46–49]. It should be noted that the intensity, width, and position of reflections are significantly different depending on the procedure used for the mesoporous silica aging and synthesis route. The estimated wall thickness (Table 2) for the SBA-15 materials is in the range of 4.9–5.2 nm. The determined pore size (Table 3) for the sample prepared according to synthesis procedure B is significantly larger in comparison to other samples. The obtained results are in accordance with the data reported in the literature (i.e., increased temperature results in formation of larger pores) [50]. However, hydrothermal conditions cause an even larger increase in pore size. Silica with grafted functional groups is characterized by smaller pore size and thicker pore walls, which has also been proven in the publication by Majda et al. [51]. According to Wang et al. [52], 2D-hexagonal ordering has been retained after post-synthesis grafting, which was also observed in the presented studies. The ^1H NMR spectra of the anchoring compounds (Supporting Material, Figures S2 and S3; Table S3) further support the successful formation of AmS and AmBenS.

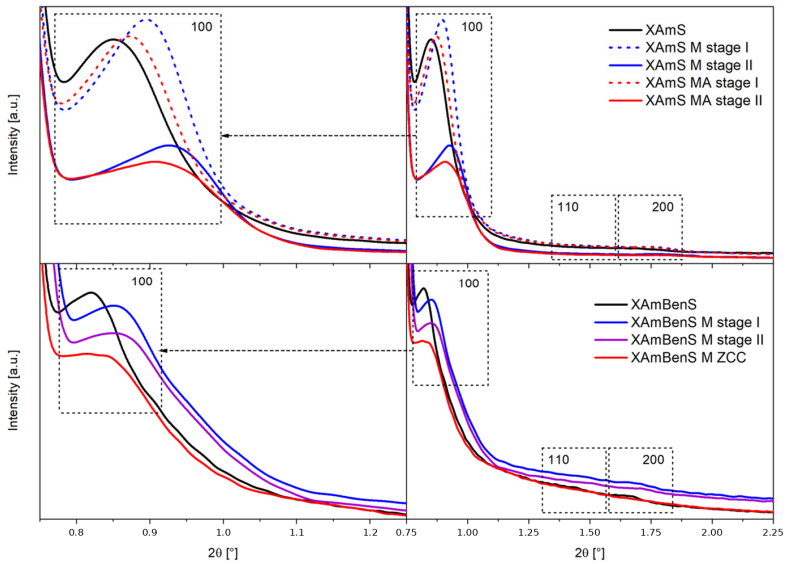

Figure 5. XRD monitoring of organo-functionalized SBA-15 adsorbents extraction.

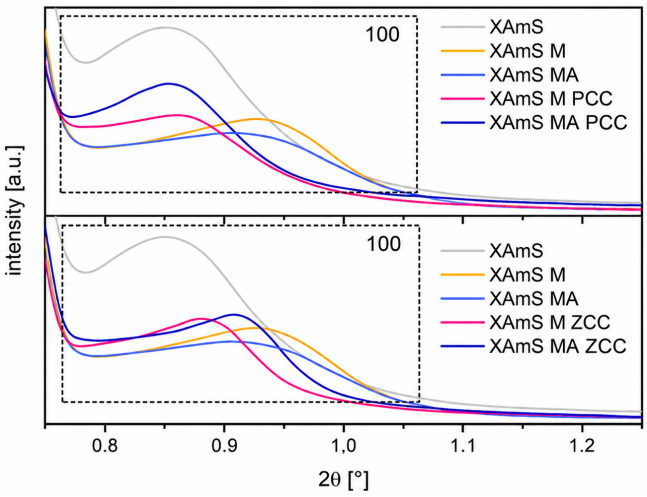

Figure 6. XRD patterns of fresh, extracted, and spent XAmS adsorbents.

Table 3. Porosity indicators obtained via thermoporometry measurements on silicas, organo-functionalized silicas before and after calcination, and after copper salt adsorption.

Sample Name	D [nm]	V [cm^3/g]
A (calcined)	6.7	0.46
AAmBenS	4.8	0.15
AAmBenS (calcined)	6.3	0.43
AAmBenS + $CuCl_2$	4.9	0.11
AAmBenS + $Cu(CH_3COO)_2$	4.8	0.13
B (calcined)	7.6	0.57
BAmS	6.2	0.26
BAmS (calcined)	7.2	0.52
BAmS + $CuCl_2$	6.2	0.28
BAmS + $Cu(CH_3COO)_2$	6.3	0.30

The extraction-monitoring series (Figure 5) provides a complementary view of the same structural trends. Complementary FT-IR data for the fresh, extracted, and metal-treated organo-functionalized silicas are presented in Figure S5. For both XAmS and XAmBenS, the (100) reflection loses intensity and broadens progressively from the as-synthesized material through stage I to stage II of Soxhlet purification, indicating a real, if modest, loss of long-range mesostructural order as the P123 template is removed, rather than a simple dilution effect from washing. This loss is more pronounced for the methanol-only extraction (M) than for the methanol/acetic acid route (MA): at stage II, the MA samples retain visibly more (100) intensity than their M counterparts, suggesting the acid-assisted extraction is gentler on the framework, plausibly because it more completely removes residual template rather than leaving it to be mechanically stripped by methanol alone.

A further, less expected pattern appears in Figure 6 and Table 2: after the multi-metal adsorption step (PCC/ZCC), the (100) reflection shifts back toward lower 2θ relative to the freshly-extracted (stage II) material; for example, a_0 for XAmS(M) rises from 11.0 nm (extracted) to 11.9 nm (PCC) and 11.6 nm (ZCC), approaching the as-synthesized value of 12.0 nm. The peaks remain broader than in the pristine material, so this is not a simple reversal of the extraction-induced disordering, but it does indicate that the framework partially re-expands on prolonged aqueous exposure (18 h contact), most likely via hydration/swelling of the silica walls rather than any metal-templating effect, since the same partial-recovery pattern is observed for both the PCC and ZCC systems despite their different metal content. Additional XRD patterns of the spent organo-silica adsorbents are provided in Figure S7.

Thermoporometry provides a second, largely independent line of evidence, and for the unmodified parent silicas it agrees well with XRD: B (calcined) shows both a larger pore diameter (7.6 vs. 6.7 nm) and larger pore volume (0.57 vs. 0.46 cm^3/g) than A, mirroring the larger unit-cell parameter seen by XRD (a_0 = 11.1 vs. 10.4 nm) (Figure 7).

Complementary N_2 adsorption/desorption isotherms and pore-size distributions are presented in Figures S8 and S9, respectively, while the corresponding BET and pore-volume parameters are compiled in Table S5. The observed isotherm profiles are characteristic of mesoporous materials with relatively uniform pore-size distributions [53]. The grafting-vs-calcination comparison in Table 3 further demonstrates that the organic ligand physically occupies pore space: as-grafted AAmBenS shows a pore diameter of only 4.8 nm and a volume of 0.15 cm^3/g, but calcining it back off recovers 6.3 nm and 0.43 cm^3/g, close to

(though not quite matching) the 6.7 nm/0.46 cm^3/g of the never-grafted parent. The same pattern holds for BAmS (6.2 → 7.2 nm; 0.26 → 0.52 cm^3/g against a 7.6 nm/0.57 cm^3/g parent), but the relative pore-diameter reduction on grafting is smaller for BAmS (~18%) than for AAmBenS (~28%), consistent with the bulkier aminobenzothiazole ligand occupying proportionally more of the pore space than the aminothiazole ligand.

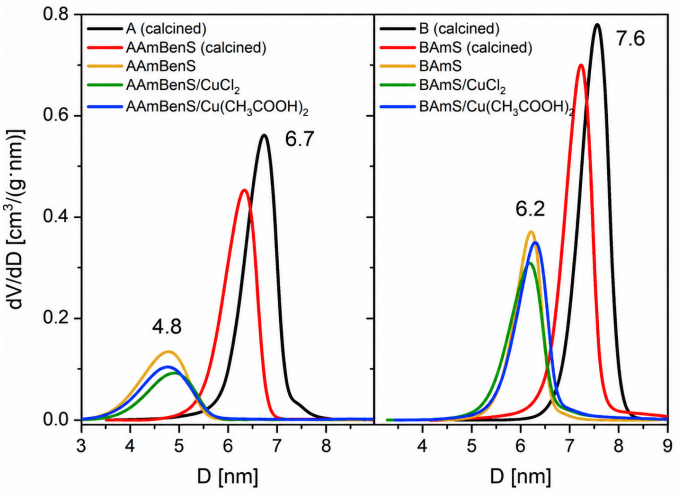

Figure 7. Pore size distribution for parent calcined SBA-15, organo-functionalized silicas before and after calcination and after copper salt adsorption.

Copper adsorption itself perturbs the two materials differently. TPM shows that $CuCl_2$ and $Cu(CH_3COO)_2$ exposure barely change BAmS's pore metrics (D and V essentially unchanged, 6.2 nm and 0.26–0.30 cm^3/g throughout) but measurably shrink AAmBenS's pore volume (0.15 → 0.11–0.13 cm^3/g) at an unchanged pore diameter, despite AAmBenS adsorbing markedly less copper than BAmS under the same single-metal conditions (Section 3.3.1, Table 4). This suggests the small amount of copper AAmBenS does capture is deposited in a way that measurably obstructs its already-narrow pores, whereas BAmS's wider channels accommodate a larger absolute Cu uptake with comparatively little volumetric consequence, a structural explanation for why pore geometry, and not only ligand density, may be limiting AAmBenS's practical capacity.

The clearest correlation between the two techniques is, in fact, a quantifiable disagreement, and it is worth stating explicitly rather than smoothing over. The wall-thickness column in Table 2 ($W = a_0 - D$) can be computed by pairing the (non-calcined) grafted-sample XRD lattice parameter with either the non-calcined or the calcined TPM pore diameter, and the two routes disagree substantially: 4.7 vs. 3.7 nm for BAmS, and 5.4 vs. 3.9 nm for AAmBenS, against a third, directly measured (D_{BJH}) calcined value of ~5.3 nm for both. A spread of 1.5–1.7 nm on a wall that is nominally 4–5 nm thick (35–45% relative) is therefore most plausibly methodological in origin rather than indicative of a real difference in silica-wall thickness: it arises from combining a room-temperature, water-swollen TPM pore size with a dry XRD lattice parameter measured on a sample of a different thermal history (organic-laden vs. calcined), which is not a self-consistent pairing. By contrast, the clean agreement between XRD and TPM for the two unmodified, matched-state parent silicas, both techniques rank B > A in pore size, with proportionally similar margins, confirms that the two methods are fundamentally consistent with one another, and that the wall-thickness discrepancy is specifically a consequence of mixing calcination states rather than a disagreement between XRD and TPM as such. Future reporting of W should therefore be restricted to same-state comparisons, or the mixed-state values should be flagged as approximate.

Table 4. Adsorption capacity of pollutants (q_e), adsorption efficiency (R_{ads}), and percentage of occupied functional groups.

Sample (Experimentally Determined Ligand Loading [mmol g^{-1}]) /Adsorbate	q_e [mmol g^{-1}]	q_e [mg g^{-1}]	R_{ads} [%]	Percentage of Occupied Functional Groups [a] [%]
BAmS (1.59–1.17 [b]) /$CuCl_2$	0.214	13.6	13	13–18
/$Cu(CH_3COO)_2$	0.607	38.6	38	38–52 [b]
AAmBenS (1.15–0.89 [b]) /$CuCl_2$	0.029	1.8	2	3
/$Cu(CH_3COO)_2$	0.087	5.5	7	8–10 [b]
Reference materials				
SBA-15 aminopropyl/Cu^{2+} [54] propyl ethylenediamine /Cu^{2+}	0.82 0.35	52.1 22.2	x	x
SBA-16 cyclam mono-/Cu^{2+} di-/Cu^{2+} tetra-sylilated/Cu^{2+} [54]	0.30 0.13 0.03	19.1 8.3 1.9	x	x
SBA-15 N-propylsalicylaldimine/ Cu^{2+} [54]	0.73	46.4	x	x

[a] assuming ligand/adsorbate binding molar ratio equal to 1:1, [b] ligand loading estimated from CHNS analysis, with the first value based on nitrogen and the second on sulfur content.

3.3. Metal Recovery and Water Cycling

3.3.1. Copper Adsorption on Organomodified SBA-15 Sorbents

Table 4 summarizes the Cu uptake measured after the 2.5 h contact period from single-metal chloride and acetate solutions on the two grafted sorbents evaluated individually, BAmS and AAmBenS, alongside representative Cu-selective SBA-15 adsorbents reported in the literature. Under the short-contact-time conditions used for this preliminary test (25 mg adsorbent, 10 mL of 1 mmol/L Cu^{2+}, 2.5 h), both materials captured markedly more copper from the acetate salt than from the chloride salt: q_e rose from 0.214 to 0.607 mmol/g for BAmS (13% → 38% removal) and from 0.029 to 0.087 mmol/g for AAmBenS (2% → 7% removal). Expressed relative to the experimentally determined CHNS-based ligand loading of each material—1.59/1.17 mmol g^{-1} (N-/S-based) for BAmS and 1.15/0.89 mmol g^{-1} for AAmBenS—corresponding to approximately 18–32% of the nominal 5 mmol g^{-1} synthesis target (Supplementary Material, Table S4), this corresponds to 13–52% and 3–10% of the available functional groups being engaged, respectively. This substantial difference between nominal and experimentally determined ligand loading indicates that only a fraction of the ligand introduced during synthesis was retained in the final material. The present experiments do not allow the relative contributions of incomplete incorporation and losses during post-synthesis treatment to be quantified. The experimentally determined ligand loading was therefore used as the relevant basis for interpreting functional-group utilization and adsorption performance. The underlying CHNS-derived ligand loadings and calculated surface coverages are summarized in Supporting Material, Table S4.

Two observations follow. First, BAmS engaged a substantially larger share of its (already limited) ligand inventory than AAmBenS under these conditions, suggesting the thiazole ligand is kinetically more accessible to Cu^{2+} at short contact times than the bulkier benzothiazole ligand, even though the competitive multi-metal screening discussed in Section 3.3.2 shows the opposite capacity ranking once the system is allowed under the

extended 18 h contact conditions. This points to a kinetic rather than thermodynamic origin for the low apparent capacity measured here: the 2.5 h contact time used for this single-metal test is short relative to the 18 h used in the multi-metal experiments, and the accompanying UV–vis-DRS and FT-IR data (Supplementary Material, Figures S4–S6) show no measurable spectral shift attributable to ligand/metal coordination, consistent with the system not having reached equilibrium. Second, both materials remain well below the uptake reported for comparable Cu-selective SBA-15 adsorbents; aminopropyl- and N-propylsalicylaldimine-functionalized SBA-15 report q_e values of 0.82 and 0.73 mmol/g, respectively [54], consistent with the substantially incomplete, and per CHNS analysis partially degraded, ligand grafting achieved here (Table S4), rather than with an intrinsic limitation of the aminothiazole/aminobenzothiazole chemistry itself.

3.3.2. Screening of Adsorption Performance of the Organomodified SBA-15 Sorbents

In contrast to the short single-metal Cu test above, the multi-metal screening (Section 2.7.2) used an extended 18 h contact period and was carried out in controlled competitive ternary mixtures selected on the basis of the metal composition observed in the soil-washing leachates described in Section 3.1: a Pb–Cd–Cu acetate system (PCC) and a Zn–Cd–Cu chloride system (ZCC), each at a nominal 0.5 mmol/L per metal, plus a higher-loading ZCC variant (2.5 mmol/L Zn). The synthetic mixtures were used to isolate competitive adsorption effects under reproducible conditions rather than to reproduce the full chemical complexity of the authentic leachates. Table 5 summarizes the triplicate-averaged removal efficiency (R, %) obtained for each metal, matrix, and sorbent.

Table 5. Removal efficiency (R, %; mean of triplicates) for each metal/matrix combination at 0.5 mmol/L per metal.

Sorbent	Pb (PCC)	Cd (PCC)	Cu (PCC)	Zn (ZCC)	Cd (ZCC)	Cu (ZCC)
AAmBenS (grafted)	96.4	96.5	97.2	96.7	96.4	96.6
XAmBenS(M) (co-cond.)	97.0	96.6	97.0	96.0	96.5	97.1
BAmS (grafted)	63.5	70.8	89.0	64.2	66.6	80.2
XAmS(M) (co-cond.)	62.8	69.8	89.8	65.1	65.9	77.9
XAmS(MA) (co-cond.)	63.1	70.1	90.0	66.1	65.9	79.3

The five sorbents separate into two clearly distinct performance groups. The aminobenzothiazole-functionalized materials (AAmBenS, grafted, and XAmBenS(M), co-condensed) removed 96.0–97.2% of every metal in both matrices, essentially independent of metal identity, counter-ion (acetate vs. chloride), or the presence of a fourth competing cation. The aminothiazole-based materials (BAmS, XAmS(M), XAmS(MA)) performed markedly worse and non-uniformly across metals: 63–63% for Pb, 66–71% for Cd and Zn, and 78–90% for Cu.

Two conclusions follow. First, the benzothiazole-extended ligand provides a substantially stronger, less metal-selective binding site than the simple thiazole ring: expressed on a molar basis, the AmBenS-family sorbents captured 1.13–1.25 mmol/g of total metal across the ternary systems, roughly 20–45% more than the AmS-family sorbents (0.83–0.93 mmol/g), despite carrying a comparable or even lower experimentally

determined ligand loading (Table S4), suggesting that the higher uptake is not explained solely by a higher site density. Second, within the aminothiazole family, removal efficiency does not distinguish the grafted material (BAmS) from the co-condensed ones (XAmS(M), XAmS(MA)): the three sorbents overlap within experimental error for every metal/matrix combination, indicating that for this ligand the synthesis route (grafting vs. co-condensation) is a secondary factor compared with the identity of the ligand itself—consistent with the similar actual grafting densities obtained for the three materials by CHNS (Table S4).

Raising the Zn feed concentration five-fold (0.5 → 2.5 mmol/L) increased Zn uptake proportionally (q_e rising from ~17 to ~79 mg/g) while removal efficiency stayed essentially unchanged (64–66%), and Cd/Cu removal on the same sorbents shifted by no more than a few percentage points, indicating that none of the three aminothiazole-based sorbents were close to saturation even at the highest metal loading tested. The adsorption experiments should nevertheless be interpreted as controlled model-system experiments rather than direct validation with authentic soil-washing effluents. The actual soil-washing experiments established the relevant metal concentration ranges and showed the strong predominance of Zn in the resulting leachates, whereas the subsequent synthetic systems allowed the competitive behavior of selected metal combinations to be examined independently of the variable background chemistry of individual soil extracts. Direct testing with authentic leachates would additionally account for matrix components such as major ions, dissolved organic matter, and residual washing reagents, and is therefore required for further validation of the process under realistic conditions.

3.3.3. Metal Selectivity and the Role of the Competing-Ion Matrix

To move beyond the qualitative comparison above, a distribution coefficient was calculated for each metal/sorbent/matrix combination on a molar basis, $K_D = q_e/C_e$, and pairwise selectivity factors $\alpha_{i/j} = K_{D,i}/K_{D,j}$ were derived for every metal pair present in each ternary system (Table 6).

Table 6. Pairwise selectivity factors ($\alpha = K_{D,i}/K_{D,j}$) calculated from the screening data in Table 5, averaged within each sorbent family.

System	Pair	AmS-Type α (Mean ± SD)	AmBenS-Type α (Mean ± SD)
PCC (Pb–Cd–Cu)	Cu/Pb	5.03 ± 0.34	1.14 ± 0.19
PCC	Cd/Pb	1.38 ± 0.01	0.95 ± 0.09
PCC	Cd/Cu	0.27 ± 0.02	0.84 ± 0.06
ZCC (Zn–Cd–Cu)	Cu/Zn	2.07 ± 0.07	1.17 ± 0.27
ZCC	Cd/Zn	1.14 ± 0.03	1.03 ± 0.15
ZCC	Cd/Cu	0.55 ± 0.01	0.89 ± 0.08

The aminothiazole-type sorbents show genuine, reproducible selectivity: Cu is bound roughly five-fold more strongly than Pb and about two-fold more strongly than Zn, an order that persists essentially unchanged when the Zn loading is raised five-fold, confirming that this is a ligand property rather than a loading artifact. The aminobenzothiazole-type sorbents, by contrast, are essentially non-selective, with every pairwise α falling within roughly ±20% of unity in both matrices, turning the qualitative observation in Section 3.3.2 ("all metals removed to a similar extent") into a quantitative, defensible claim.

Notably, the sign of the AmS-family's molar preference reverses between matrices: Cd > Cu > Pb in the acetate-based PCC system (Cd/Cu = 0.27, i.e., Cu is preferred over Cd),

but Cu > Cd ≈ Zn in the chloride-based ZCC system. This is consistent with competitive aqueous-phase complexation of Pb^{2+} and Cu^{2+} by acetate, which would lower their free-ion activity, and hence their availability for surface complexation, relative to the more weakly acetate-complexed Cd^{2+}; in the chloride matrix, where such complexation is comparatively weak for all four metals, Cu^{2+} instead shows the highest molar affinity, plausibly reflecting its favorable coordination geometry with the thiazole N/S donor set. These remain working hypotheses that would benefit from complementary aqueous-speciation modeling or single-metal reference experiments.

3.3.4. Adsorption–Desorption Cyclability and Reusability

The two best-performing co-condensed sorbents, XAmS(M) and XAmBenS(M), were carried through five adsorption/desorption cycles (Section 2.7.3) using 0.01 M HCl as the regenerating eluent. These five-cycle experiments assess sorbent reusability and regeneration stability and do not represent repeated washing cycles of the soil itself. Table 7 summarizes the cumulative metal uptake, cumulative metal recovered, and overall retention over the full five-cycle sequence; Figure 8 shows the per-cycle removal efficiency trend for each metal as well as desorption potential.

Table 7. Cumulative metal uptake, cumulative metal recovered by 0.01 M HCl elution, and overall cumulative recovery over five adsorption/desorption cycles.

Sorbent	Matrix	Metal	$Q_{cum,ads}$ (mg/g)	$Q_{cum,des}$ (mg/g)	Cumulative Recovery (%)
XAmBenS(M)	PCC	Pb	403.1	1.85	0.46
XAmBenS(M)	PCC	Cd	213.8	0.14	0.07
XAmBenS(M)	PCC	Cu	113.8	0.34	0.30
XAmS(M)	PCC	Pb	338.7	1.03	0.31
XAmS(M)	PCC	Cd	188.6	0.13	0.07
XAmS(M)	PCC	Cu	109.4	12.10	11.07
XAmBenS(M)	ZCC	Zn	147.5	0.29	0.20
XAmBenS(M)	ZCC	Cd	210.5	0.14	0.07
XAmBenS(M)	ZCC	Cu	127.1	0.39	0.31
XAmS(M)	ZCC	Zn	125.6	0.41	0.33
XAmS(M)	ZCC	Cd	179.7	0.57	0.32
XAmS(M)	ZCC	Cu	112.3	4.92	4.39

XAmBenS(M) showed outstanding operational stability. Removal efficiency for Pb, Cd, and Cu stayed within a narrow 96.0–98.0% band across all 5 cycles in both matrices (maximum drop of 1.4 percentage points between cycle 1 and cycle 5). XAmS(M) behaved differently and metal-specifically. Pb and Cd removal did not decline at all: both increased slightly over the five cycles (Pb: 80.2% → 81.7%; Cd: 84.0% → 86.3%, PCC matrix), while Cu removal fell steadily and substantially, from 96.8% to 89.0% in the PCC matrix (a 7.8-percentage-point, ~8% relative loss) and from 88.5% to 84.9% in the ZCC matrix, indicating progressive fatigue of the Cu-binding sites specifically on the aminothiazole sorbent.

This selective fatigue is corroborated by the desorption data. Cu was also the metal desorbed most efficiently from XAmS(M) at every cycle (15.8% of the adsorbed Cu recovered in cycle 1, falling to 6.9% by cycle 5), whereas Pb and Cd were desorbed only marginally (≤1.0% per cycle) throughout. On XAmBenS(M), desorption of all three metals—including

Cu—remained below 1% per cycle throughout, i.e., essentially irreversible under the 0.01 M HCl elution used. These results also demonstrate that adsorption-capacity retention and regeneration efficiency are not equivalent parameters. Substantial adsorption performance may be retained while a large fraction of the previously adsorbed Cu remains associated with the sorbent. Cumulatively, over the whole five-cycle sequence, only 11.1% (PCC) and 4.4% (ZCC) of the Cu taken up by XAmS(M) was ever recovered by the eluent, versus 0.30–0.31% for XAmBenS(M) (Table 7); Pb, Cd, and Zn were essentially fully retained (>99.5% cumulative retention) on both sorbents regardless of matrix. The complete cycle-by-cycle calculation framework used to derive desorption efficiency, retained metal, and reversible/retained fractions is given in Supporting Material, Section S3.

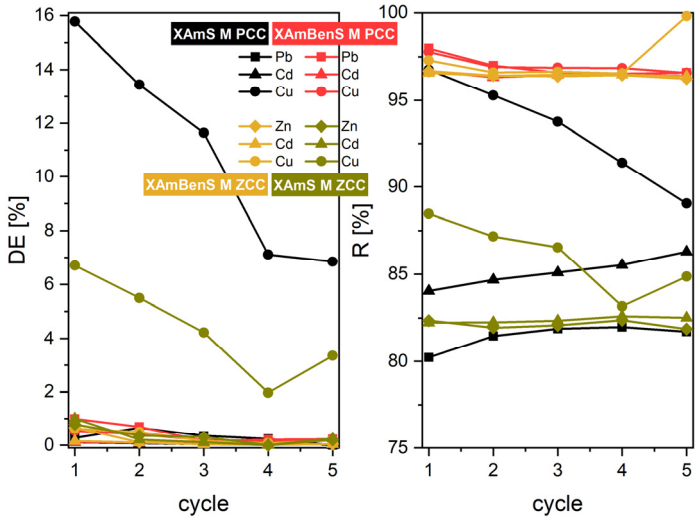

Figure 8. Removal efficiency (R, %) over five consecutive adsorption cycles for XAmBenS(M) and XAmS(M) in the synthetic ternary PCC (Pb–Cd–Cu, acetate) and ZCC (Zn–Cd–Cu, chloride) model systems, together with per-cycle desorption efficiency (DE, %) of Cu from XAmS(M) and XAmBenS(M), illustrating the greater reversibility of Cu binding on the aminothiazole sorbent.

Taken together with the screening and selectivity results (Sections 3.3.2 and 3.3.3), these cycling data support a two-tier sorbent strategy consistent with the closed-loop scheme proposed in Figure 1. XAmBenS(M) (and, by extension, its grafted analog AAmBenS) is best suited to a polishing/immobilization step that drives residual metal concentrations to very low levels and can be reused many times without measurable loss of capacity, closing the water loop by returning a near metal-free effluent for reuse or safe discharge. XAmS(M) (and BAmS), while less efficient overall and subject to gradual Cu-specific capacity loss on cycling, uniquely combines strong retention of Pb/Cd/Zn with partial Cu reversibility, resulting in measurable Cu release into the regenerant under the applied 0.01 M HCl conditions and providing a potential basis for selective Cu recovery. Realizing higher overall recovery yields for Cu, or extending selective recovery to Pb, Cd, and Zn, would likely require a dedicated regeneration chemistry optimized independently of the adsorption step, since the present dataset, built around a single fixed elution protocol, cannot establish whether the low desorption of Pb, Cd, and Zn reflects an intrinsic binding limit or an eluent choice not yet optimized for recovery.

3.3.5. Statistical Evaluation of Cycling Trends

The single-run screening experiments (Sections 3.3.2 and 3.3.3) were performed in triplicate ($n = 3$); the five-cycle regeneration study (Section 3.3.4) was performed once per sorbent/metal/matrix combination, since each cycle depends sequentially on the sorbent

state left by the previous one. To place the reusability trends reported in Section 3.3.4 on a formal statistical footing despite this constraint, we treated each sorbent/metal combination's five sequential capacity-retention values (CR_n, normalized to cycle 1 = 100%) as a repeated-measures series and tested, by linear regression against cycle number (Table 8, Figure S10), whether the observed trend differs significantly from a flat (zero-slope) response. This tests whether the change across cycles is statistically supported, independent of the question of triplicate precision within any single cycle.

Table 8. Linear regression of capacity retention (CR_n) against cycle number (n = 5 cycles per combination), with cumulative uptake and desorption metrics from Table 7 for reference.

Sorbent/ Matrix	Metal	CR_5 (%)	Slope (%/Cycle)	95% CI	R^2	p-Value	Significant?	$Q_{cum,ads}$ (mg/g)	DE, Summed over 5 Cycles (%)
XAmBenS(M), PCC	Pb	98.6	−0.33	±0.39	0.70	0.077	No	403.1	2.28
XAmBenS(M), PCC	Cd	99.7	−0.04	±0.14	0.24	0.397	No	213.8	0.33
XAmBenS(M), PCC	Cu	98.8	−0.25	±0.28	0.73	0.067	No	113.8	1.50
XAmBenS(M), ZCC	Zn	99.5	−0.09	±0.10	0.71	0.071	No	147.5	1.00
XAmBenS(M), ZCC	Cd	99.8	−0.03	±0.07	0.43	0.228	No	210.5	0.33
XAmBenS(M), ZCC	Cu	102.6	+0.51	±1.37	0.32	0.320	No	127.1	1.54
XAmS(M), PCC	Pb	101.9	+0.44	±0.66	0.60	0.124	No	338.7	1.53
XAmS(M), PCC	Cd	102.7	+0.64	±0.13	0.99	0.0006	Yes	188.6	0.35
XAmS(M), PCC	Cu	92.0	−2.00	±0.43	0.99	0.0007	Yes	109.4	54.83
XAmS(M), ZCC	Zn	99.4	−0.07	±0.30	0.14	0.537	No	125.6	1.65
XAmS(M), ZCC	Cd	100.3	+0.11	±0.11	0.77	0.050	Borderline	179.7	1.58
XAmS(M), ZCC	Cu	95.9	−1.27	±1.39	0.74	0.063	Borderline	112.3	21.75

Two conclusions follow. First, every trend measured for XAmBenS(M) is statistically indistinguishable from zero ($p \geq 0.067$ in all cases), formally supporting the claim that this sorbent's performance is stable across five reuse cycles, rather than relying on the values' visual proximity to 100% alone. Second, XAmS(M) shows two clearly significant trends: a declining copper capacity (slope = −2.00%/cycle, $p = 0.0007$) and, less expected, a small but statistically real increase in cadmium retention (slope = +0.64%/cycle, $p = 0.0006$); the corresponding declines in copper capacity and desorption efficiency in the chloride matrix, and the increase in Pb retention, fall short of the conventional 0.05 threshold ($p = 0.05$–0.12) and should be treated as suggestive trends pending further replication rather than confirmed effects.

We emphasize that this analysis tests the significance of the trend within the single cycling run performed for each condition; it does not substitute for independent triplicate repetition of the full five-cycle protocol, which remains a priority for a follow-up, pilot-scale validation of the reusability claims made here.

4. Mass Balance and Circularity Evaluation

4.1. Basis

All figures below use a functional unit of 1 ton of soil and a modeled upper-bound leachate composition constructed from the individual maximum metal concentrations measured in the acetic acid leachates reported in Table 1, processed under the conditions validated in Section 2.2 (soil washing, 1:10 solid/liquid, 0.01 M acetic acid) and Section 2.7 (adsorption and regeneration, 10 mg sorbent: 9 mL solution, 0.01 M HCl elution), for the two sorbents representing our two-tier treatment strategy (Section 3.3.4, Figure 1): the non-selective, high-capacity XAmBenS(M), and the copper-selective XAmS(M). Because no single experiment tested all four target metals together, removal and desorption efficiencies were mapped from the closest-matching competitive system: Pb from the Pb–Cd–Cu acetate (PCC) system, and Cd, Zn, Cu from the Zn–Cd–Cu chloride (ZCC) system, since Zn, the dominant mass fraction of the real leachate, was only tested there. This mapping is a modeling assumption, revisited in Section 4.4.

4.2. Soil Washing and Single-Pass Adsorption Treatment

Extrapolation of the experimentally determined soil-washing data to 1 t of soil at 1:10 (m/V) gives an estimated consumption of 10 m^3 of 0.01 M acetic acid (6.0 kg CH_3COOH) and mobilization of 324.9 g of total metal into the leachate, overwhelmingly zinc (320.0 g, 98.5% of the total; Cd 2.7 g, Pb 2.0 g, Cu 0.2 g). Treating this leachate at the solid/liquid ratio validated in Section 2.7 requires 11.11 kg of adsorbent (identical for both sorbents) and 10 m^3 of 0.01 M HCl (3.65 kg) for the paired regeneration step. Table 9 summarizes the resulting single-pass performance and residual water quality.

Table 9. Modeled single-pass mass balance per tonne of soil treated, based on the individual maximum acetic acid leachate concentrations reported in Table 1.

	XAmBenS(M)	XAmS(M)
Metal adsorbed (of 324.9 g leachate)	311.9 g (95.9%)	211.5 g (65.1%)
Metal residual in treated water	13.0 g (4.0%)	113.4 g (34.9%)
Cd/Pb/Zn/Cu (mg/L)	0.0095/0.006/1.28/0.0006	0.092/0.074/11.17/0.0044
Metal desorbed in paired regeneration	0.62 g	0.70 g
Net metal retained on sorbent (g; corresponding loading, mg/g))	311.3 g (28.0 mg/g)	210.8 g (19.0 mg/g)
Water balance	20 m^3 in (10 washing + 10 regeneration) = 10 m^3 treated water + 10 m^3 regenerant eluate out	same
Reagents consumed	6.0 kg AcOH + 3.65 kg HCl	same

Zinc dominates the leachate by mass, so overall treated-water quality tracks each sorbent's zinc performance rather than its (more selective) copper behavior.

4.3. Sorbent Cycle Life and Copper Recovery

Comparing the metal load estimated for a dilute-leachate pass, based on the experimentally measured soil-washing composition (Table 8), with each sorbent's saturation capacity, the cumulative total metal loading reached over five laboratory regeneration cycles (Section 3.3.4; Pb+Cd from PCC, Zn+Cu from ZCC) gives the cycle life, amortized consumption, and copper recovery reported in Table 10.

Table 10. Cycle life, amortized streams, and copper recovery.

	XAmBenS(M)	XAmS(M)
Saturation benchmark (mg total metal/g)	884.7	763.7
Cycles to saturation	≈32	≈41
Adsorbent, amortized consumption	0.35 kg/t soil	0.27 kg/t soil
Spent sorbent, secondary waste (per service life)	20.9 kg per 32 t soil (11.11 kg + 9.83 kg metal)	19.6 kg per 41 t soil (11.11 kg + 8.49 kg metal)
Cu adsorbed/desorbed, single pass	194.2 mg/0.60 mg	155.8 mg/6.78 mg
Cu adsorbed/desorbed, cumulative over service life	6.13 g/19 mg	6.27 g/273 mg

XAmS(M) requires more cycles to saturate than XAmBenS(M) despite a similar capacity ceiling, because it captures less metal per pass at real, dilute concentrations (Section 3.3.2). Both sorbents ultimately adsorb a similar total quantity of copper, but XAmS(M) releases roughly 14-fold more of it in absolute terms. These calculations indicate that XAmS(M) has greater potential for copper recovery under the modeled process conditions; however, confirmation under authentic soil-washing leachates is still required.

4.4. Limitations

The estimates above rest on assumptions that should be resolved by future work. In particular, the adsorption and regeneration experiments were performed using controlled synthetic multi-metal solutions rather than authentic soil-washing leachates. Although the synthetic mixtures were selected on the basis of the metal composition observed in the experimentally obtained soil-washing effluents, they do not reproduce the full matrix complexity of real leachates. Therefore, the present data demonstrate controlled competitive adsorption and regeneration behavior, but do not constitute complete validation of the process under authentic soil-washing conditions. A further limitation is that sequential soil-washing cycles were not experimentally investigated. Therefore, although the tested contact times provide information on the time-dependent mobilization of metals, the cumulative efficiency and feasibility of repeated washing cannot be established from the present data. Further experiments should evaluate whether successive washing steps provide sufficient additional metal removal to justify the additional consumption of washing reagent and generation of secondary effluent.

Additional limitations include (i) no single experiment tested all four metals together, so leachate-scale performance is inferred by combining the PCC and ZCC datasets; (ii) the regenerant eluate requires further downstream treatment (copper concentration, acid neutralization) not costed here; (iii) cycle life assumes constant per-cycle performance, whereas XAmS(M)'s copper desorption is observed to decline somewhat over five laboratory cycles, so its true cycle life is likely somewhat below the ≈41 estimated here; (iv) sorbent attrition over repeated handling is unmeasured; and (v) energy consumption (agitation, separation, sorbent handling) has not been metered at bench scale and requires a dedicated life-cycle assessment before techno-economic claims can be made. In addition, the synthesis efficiency of ligand incorporation and the batch-to-batch variability of the experimentally determined ligand loading were not systematically investigated. Moreover, the regenerant eluate could substantially alter the water-consumption and metal-flow balance if a more effective method for desorbing metals from the adsorbent were developed. Further research may enable the selection of a more efficient regenerant solution or mixture that can be used in a smaller volume while producing a more concentrated metal-bearing eluate.

5. Conclusions

This study addressed both halves of the closed-loop scheme proposed in Figure 1: a soil-washing step that mobilizes heavy metals into an aqueous effluent, and a sorbent-based treatment step that recovers them from it. Four conclusions follow.

1. Soil decontamination does not eliminate the problem—it shifts it.

The washing step successfully reduces the total metal content in the soil, especially at moderately contaminated sites, but the extracted metals accumulate in the liquid phase rather than disappearing. For Cd and Pb, both subject to strict regulatory thresholds, Table 1 shows that acetic acid filtrates often exceed permissible discharge concentrations.

2. Mild acids do not guarantee mild effluents.

Although acetic acid is less efficient than citric acid, Table 1 shows that the absolute metal loads it mobilizes remain environmentally relevant. This is particularly striking for Cd: even an extraction of only 5–10% can produce filtrates with concentrations that require dedicated treatment.

3. Filtrates constitute a valuable but contaminated stream.

Given the quantified ranges in Table 1, acidic leachates can be regarded as metal-rich solutions suitable for secondary purification or metal recovery. Their composition, low pH, moderate ionic strength, and a relatively simple organic matrix make them favorable for sorption-based purification, as demonstrated by the organomodified SBA-15 sorbents evaluated in Section 3.3.

4. Tailor-made adsorbents close the loop, but no single material does everything.

The two sorbent families examined offer complementary, not interchangeable, solutions to the effluent problem identified above. The aminobenzothiazole-functionalized materials (AAmBenS, XAmBenS(M)) removed 96–97% of Pb, Cd, Cu, and Zn essentially independent of matrix and retained this adsorption performance over the five tested cycles, making them well suited to driving residual metal concentrations substantially downward and potentially supporting further purification. The aminothiazole-functionalized materials (BAmS, XAmS(M)/(MA)) are markedly less efficient overall but are genuinely Cu-selective (a distribution-coefficient ratio of ~5 relative to Pb) and are the only sorbents from which a measurable fraction of the adsorbed copper, up to 11% cumulatively, was recovered in the regenerant under the applied 0.01 M HCl conditions. Thus, the aminothiazole-functionalized materials demonstrate partial Cu recoverability under the applied regeneration conditions, whereas most of the adsorbed Cu remains associated with the sorbent.

Taken together, these results show that closing the water loop in Figure 1 requires pairing these two sorbent behaviors rather than choosing between them: a non-selective, highly reusable material to purify the bulk effluent, and a selective, regenerable material to provide a potential route toward secondary Cu recovery, although further optimization of regeneration and downstream metal recovery is required. The soil-washing step should therefore be viewed not as an endpoint but as the first stage of an integrated remediation-and-recovery scheme. The present results demonstrate the potential of the investigated sorbents to provide both aqueous-phase purification and selective copper recovery under controlled model conditions, while validation using authentic soil-washing leachates remains necessary before practical process applicability can be established.

Supplementary Materials: The following supporting information can be downloaded at https://www.mdpi.com/article/10.3390/jox16070214/s1, "A_Wegrzyn_Closing_the_loop_supplementary_material.pdf", "A_Wegrzyn_RESULTS_adsorption-desorption.xlsx". Supplementary Materials' chapters: S1. Synthesis of the organic ligands and their incorporation into SBA-15; S2. Characterization of materi-

als; S3. Calculations for the adsorption-desorption cycling parameters. Figures: Figure S1. FT-IR spectra of ICPTES modified with selected functional groups (2-aminothiazole and 2-aminobenzothiazole), corresponding to the anchoring compounds AmS and AmBenS. Figure S2. ^1H NMR spectrum of 1-(1,3-thiazol-2-yl)-3-(3-triethoxysilylpropyl)urea (AmS). Figure S3. ^1H NMR spectrum of 1-(1,3-benzothiazol-2-yl)-3-(3-triethoxysilylpropyl)urea (AmBenS). Figure S4. UV-Vis diffuse reflectance spectra (UV-Vis-DRS) of solid and liquid components of the adsorption mixtures used for copper remediation. Figure S5. FT-IR spectra of organo-functionalised silica materials in their fresh state, after extraction, and after adsorption of lead, cadmium, and copper. Figure S6. FT-IR spectra of starting organic ligands, silica materials modified with organic functional groups, and adsorbents after soaking in copper acetate solution. Figure S7. XRD patterns of spent organo-silica adsorbents after adsorption and extraction experiments. Figure S8. Nitrogen adsorption-desorption isotherms of calcined SBA-15 materials: (A) pristine silica supports prepared using different synthesis procedures; (B) silica materials after grafting with organofunctional groups. Figure S9. Pore size distributions of calcined SBA-15 materials: (A) pristine silica supports prepared using different synthesis procedures; (B) silica materials after grafting with organofunctional groups. Figure S10. Linear regression of capacity retention (CR_n) as a function of cycle number for different adsorbents and metal-containing matrices: (A) XAmBenS M in ZCC; (B) XAmS M in ZCC; (C) XAmBenS M in PCC; and (D) XAmS M in PCC. The individual plots show the changes in capacity retention for the respective metals (Pb, Cd, Cu or Zn, depending on the matrix). Tables: Table S1. Chemical structures and formulas of the starting materials and reaction products, together with the abbreviations of the synthesised anchoring compounds. Table S2. FT-IR peak assignments for the anchoring compounds AmS and AmBenS. Table S3. ^1H NMR chemical shifts and signal multiplicities assigned to the anchoring compounds AmS and AmBenS. Table S4. Elemental composition and surface density of organofunctional groups on SBA-15 materials, including obtained and theoretically expected values of organosilane surface coverage. Table S5. Textural parameters of pristine SBA-15 supports and organofunctionalised materials determined by low-temperature nitrogen adsorption, including BET surface area, microporous and mesoporous surface areas, external surface area, BJH mesopore diameter, and pore volumes. Additional Supplementary File: Supplementary File ADSORPTION-DESORPTION.XLSX. Experimental adsorption and desorption data and calculated adsorption-desorption cycling parameters for the investigated organo-functionalised silica adsorbents. The workbook includes single-run adsorption experiments, five-cycle adsorption-desorption experiments, and statistical parameters describing capacity retention and adsorption-desorption performance.

Author Contributions: Conceptualization, A.W. and P.M.; methodology, A.W., D.C., P.M. and D.M.; formal analysis, A.W.; investigation, P.M., A.W., A.K., M.R.-Z., D.C., D.M. and X.T.D.; data curation, A.K. and P.M.; writing—original draft preparation, A.W. and P.M.; writing—review and editing, P.M. and A.W.; supervision, A.W., P.M. and D.C. All authors have read and agreed to the published version of the manuscript.

Funding: The study was partially carried out using research infrastructure funded by the European Union in the framework of the Smart Growth Operational Programme, Measure 4.2; Grant Number POIR.04.02.00-00-D001/20, "ATOMIN 2.0—Center for materials research on ATOMic scale for the INnovative economy".

Institutional Review Board Statement: Not applicable.

Informed Consent Statement: Not applicable.

Data Availability Statement: The original contributions presented in this study are included in the article/Supplementary Material. Further inquiries can be directed to the corresponding authors.

Conflicts of Interest: The authors declare no conflicts of interest.

References

1. Xu, L.; Zhao, F.; Xing, X.; Peng, J.; Wang, J.; Ji, M.; Li, B.L. A Review on Remediation Technology and the Remediation Evaluation of Heavy Metal-Contaminated Soils. *Toxics* **2024**, *12*, 897. [CrossRef] [PubMed]
2. Raffa, C.M.; Chiampo, F.; Shanthakumar, S. Remediation of Metal/Metalloid-Polluted Soils: A Short Review. *Appl. Sci.* **2021**, *11*, 4134. [CrossRef]

3. Wuana, R.A.; Okieimen, F.E. Heavy Metals in Contaminated Soils: A Review of Sources, Chemistry, Risks and Best Available Strategies for Remediation. *ISRN Ecol.* **2011**, *2011*, 402647. [CrossRef]
4. Kabata-Pendias, A. *Trace Elements in Soils and Plants: Fourth Edition*; CRC Press: Boca Raton, FL, USA, 2010; ISBN 9781420093704.
5. Saleem, M.; Pierce, D.; Wang, Y.; Sens, D.A.; Somji, S.; Garrett, S.H. Heavy Metal(Oid)s Contamination and Potential Ecological Risk Assessment in Agricultural Soils. *J. Xenobiotics* **2024**, *14*, 634–650. [CrossRef] [PubMed]
6. Correia, A.A.S.; Rasteiro, M.G. A Review of Persistent Soil Contaminants: Assessment and Remediation Strategies. *Environments* **2025**, *12*, 229. [CrossRef]
7. Vogiantzi, C.; Tserpes, K. On the Definition, Assessment, and Enhancement of Circular Economy across Various Industrial Sectors: A Literature Review and Recent Findings. *Sustainability* **2023**, *15*, 16532. [CrossRef]
8. Geissdoerfer, M.; Savaget, P.; Bocken, N.M.P.; Hultink, E.J. The Circular Economy—A New Sustainability Paradigm? *J. Clean. Prod.* **2017**, *143*, 757–768. [CrossRef]
9. Rodríguez-Rasero, C.; Garrido-Zoido, J.M.; García-Galán, M.d.M.; Cuerda-Correa, E.M.; Alexandre-Franco, M.F. Coffee Waste as a Green Precursor for Iron Nanoparticles: Toward Circular, Efficient and Eco-Friendly Dye Removal from Aqueous Systems. *J. Xenobiotics* **2025**, *15*, 158. [CrossRef] [PubMed]
10. Ostellari, P.; Gross, S. A Mature Tool to Address New Challenges: Harnessing Coordination Chemistry for The Sustainable Copper Recovery from Industrial and E-Waste in The Age of Energy Transition. *Eur. J. Inorg. Chem.* **2025**, *28*, e202400704. [CrossRef]
11. Valenta, R.K.; Kemp, D.; Owen, J.R.; Corder, G.D.; Lèbre, É. Re-Thinking Complex Orebodies: Consequences for the Future World Supply of Copper. *J. Clean. Prod.* **2019**, *220*, 816–826. [CrossRef]
12. Biancardi, A.; D'Adamo, I.; Santibanez-Gonzalez, E.D.R.; Bascur, J.F.V. A Flexible and Circular Management of Copper in Chile: New Perspectives Toward Sustainable Development. *Glob. J. Flex. Syst. Manag.* **2025**, *26*, 813–837. [CrossRef]
13. Elshkaki, A.; Graedel, T.E.; Ciacci, L.; Reck, B.K. Copper Demand, Supply, and Associated Energy Use to 2050. *Glob. Environ. Chang.* **2016**, *39*, 305–315. [CrossRef]
14. Moreno-Leiva, S.; Haas, J.; Junne, T.; Valencia, F.; Godin, H.; Kracht, W.; Nowak, W.; Eltrop, L. Renewable Energy in Copper Production: A Review on Systems Design and Methodological Approaches. *J. Clean. Prod.* **2020**, *246*, 118978. [CrossRef]
15. Dang, D.H.; Thompson, K.A.; Ma, L.; Nguyen, H.Q.; Luu, S.T.; Duong, M.T.N.; Kernaghan, A. Toward the Circular Economy of Rare Earth Elements: A Review of Abundance, Extraction, Applications, and Environmental Impacts. *Arch. Environ. Contam. Toxicol.* **2021**, *81*, 521–530. [CrossRef] [PubMed]
16. Jowitt, S.M.; Werner, T.T.; Weng, Z.; Mudd, G.M. Recycling of the Rare Earth Elements. *Curr. Opin. Green Sustain. Chem.* **2018**, *13*, 1–7. [CrossRef]
17. Stawiński, W.; Węgrzyn, A.; Mordarski, G.; Skiba, M.; Freitas, O.; Figueiredo, S. Sustainable Adsorbents Formed from By-Product of Acid Activation of Vermiculite and Leached-Vermiculite-LDH Hybrids for Removal of Industrial Dyes and Metal Cations. *Appl. Clay Sci.* **2018**, *161*, 6–14. [CrossRef]
18. Stawiński, W.; Węgrzyn, A.; Freitas, O.; Chmielarz, L.; Mordarski, G.; Figueiredo, S. Simultaneous Removal of Dyes and Metal Cations Using an Acid, Acid-Base and Base Modified Vermiculite as a Sustainable and Recyclable Adsorbent. *Sci. Total Environ.* **2017**, *576*, 398–408. [CrossRef] [PubMed]
19. Gusiatin, Z.M.; Kulikowska, D.; Klik, B. New-Generation Washing Agents in Remediation of Metal-Polluted Soils and Methods for Washing Effluent Treatment: A Review. *Int. J. Environ. Res. Public Health* **2020**, *17*, 6220. [CrossRef] [PubMed]
20. Dermont, G.; Bergeron, M.; Mercier, G.; Richer-Laflèche, M. Soil Washing for Metal Removal: A Review of Physical/Chemical Technologies and Field Applications. *J. Hazard. Mater.* **2008**, *152*, 1–31. [CrossRef] [PubMed]
21. Liu, J.; Zhao, L.; Liu, Q.; Li, J.; Qiao, Z.; Sun, P.; Yang, Y. A Critical Review on Soil Washing during Soil Remediation for Heavy Metals and Organic Pollutants. *Int. J. Environ. Sci. Technol.* **2022**, *19*, 601–624. [CrossRef]
22. Bhattacharyya, K.G.; Gupta, S. Sen Adsorption of a Few Heavy Metals on Natural and Modified Kaolinite and Montmorillonite: A Review. *Adv. Colloid Interface Sci.* **2008**, *140*, 114–131. [CrossRef] [PubMed]
23. Wang, S.; Peng, Y. Natural Zeolites as Effective Adsorbents in Water and Wastewater Treatment. *Chem. Eng. J.* **2010**, *156*, 11–24. [CrossRef]
24. Joseph, L.; Jun, B.M.; Flora, J.R.V.; Park, C.M.; Yoon, Y. Removal of Heavy Metals from Water Sources in the Developing World Using Low-Cost Materials: A Review. *Chemosphere* **2019**, *229*, 142–159. [CrossRef] [PubMed]
25. Miśkowiec, P.; Łaptaś, A.; Zięba, K. Soil Pollution with Heavy Metals in Industrial and Agricultural Areas: A Case Study of Olkusz District. *J. Elem.* **2015**, *20*, 353–362. [CrossRef]
26. Gruszecka-Kosowska, A.; Kicińska, A. Long-Term Metal-Content Changes in Soils on the Olkusz Zn–Pb Ore-Bearing Area, Poland. *Int. J. Environ. Res.* **2017**, *11*, 359–376. [CrossRef]
27. Kicińska, A.; Smreczak, B.; Jadczyszyn, J. Soil Bioavailability of Cadmium, Lead, and Zinc in the Areas of Zn-Pb Ore Mining and Processing (Bukowno, Olkusz). *J. Ecol. Eng.* **2019**, *20*, 84–92. [CrossRef]

28. Chrastný, V.; Vaněk, A.; Teper, L.; Cabala, J.; Procházka, J.; Pechar, L.; Drahota, P.; Penížek, V.; Komárek, M.; Novák, M. Geochemical Position of Pb, Zn and Cd in Soils near the Olkusz Mine/Smelter, South Poland: Effects of Land Use, Type of Contamination and Distance from Pollution Source. *Environ. Monit. Assess.* **2012**, *184*, 2517–2536. [CrossRef] [PubMed]
29. Pasieczna, A.; Lis, J.; Górecka, E.; Dusza-Dobek, A.; Witkowska, A. *Detailed Geochemical Map of Upper Silesia 1:25000, Olkusz Map Sheet M-34-64-A-A*; Polish Geological Institute: Warsaw, Poland, 2008.
30. *ISO 10390:2005*; Soil Quality—Determination of PH. ISO: Geneve, Switzerland, 2005.
31. Ryżak, M.; Bartmiński, P.; Bieganowski, A. Methods for Determination of Particle Size Distribution of Mineral Soils. *Acta Agrophysica* **2009**, *175*, 48–51.
32. *EPA METHOD 3050B*; Acid Digestion of Sediments, Sludges and Soils. U.S. Environmental Protection Agency: Washington, DC, USA, 1996.
33. Miśkowiec, P. Spatial Distribution of Contamination With Selected Trace Metals in Mountain Soils of the Beskid Mały Mountains in Southern Poland. *Clean Soil Air Water* **2025**, *53*, e70020. [CrossRef]
34. Shi, J.; Pang, J.; Liu, Q.; Luo, Y.; Ye, J.; Xu, Q.; Long, B.; Ye, B.; Yuan, X. Simultaneous Removal of Multiple Heavy Metals from Soil by Washing with Citric Acid and Ferric Chloride. *RSC Adv.* **2020**, *10*, 7432–7442. [CrossRef] [PubMed]
35. Węgrzyn, A.; Radko, M.; Majda, D.; Stawiński, W.; Skiba, M.; Cież, D. Interaction between Adsorbed Molecules and Tailor Made Large Chelating Ligands Grafted on SBA-15 Studied by Means of Thermoporometry. *Microporous Mesoporous Mater.* **2018**, *268*, 31–38. [CrossRef]
36. Majda, D.; Zimowska, M.; Tarach, K.; Góra-Marek, K.; Napruszewska, B.D.; Michalik-Zym, A. Water Thermoporosimetry as a Tool of Characterization of the Textural Parameters of Mesoporous Materials: Refinement of the Methodology. *J. Therm. Anal. Calorim.* **2017**, *127*, 207–220. [CrossRef]
37. Landry, M.R. Thermoporometry by Differential Scanning Calorimetry: Experimental Considerations and Applications. *Thermochim. Acta* **2005**, *433*, 27–50. [CrossRef]
38. Davidova, S.; Milushev, V.; Satchanska, G. The Mechanisms of Cadmium Toxicity in Living Organisms. *Toxics* **2024**, *12*, 875. [CrossRef] [PubMed]
39. García-Ruiz, S.; Petrov, I.; Vassileva, E.; Quétel, C.R. Cadmium Determination in Natural Waters at the Limit Imposed by European Legislation by Isotope Dilution and TiO_2 Solid-Phase Extraction. *Anal. Bioanal. Chem.* **2011**, *401*, 2785–2792. [CrossRef] [PubMed]
40. European Parliament and Council of the European Union. *EU Directive 2013/39/EU of the European Parliament and of the Council of 12 August 2013 Amending Directives 2000/60/EC and 2008/105/EC as Regards Priority Substances in the Field of Water Policy*; European Parliament and Council of the European Union: Brussels, Belgium, 2013; Volume 226.
41. Onen, P.; Akemkwene, R.; Nakiguli, C.K.; Nimusiima, D.; Ruma, D.H.; Khanakwa, A.V.; Angiro, C.; Bamanya, G.; Opio, B.; Gonzaga, A.; et al. Health Risks from Intake and Contact with Toxic Metal-Contaminated Water from Pager River, Uganda. *J. Xenobiotics* **2023**, *13*, 544–559. [CrossRef] [PubMed]
42. Generalova, A.; Davidova, S.; Satchanska, G. The Mechanisms of Lead Toxicity in Living Organisms. *J. Xenobiotics* **2025**, *15*, 146. [CrossRef] [PubMed]
43. Schoofs, H.; Schmit, J.; Rink, L. Zinc Toxicity: Understanding the Limits. *Molecules* **2024**, *29*, 3130. [CrossRef] [PubMed]
44. Liao, W.; Zhu, Z.; Feng, C.; Yan, Z.; Hong, Y.; Liu, D.; Jin, X. Toxicity Mechanisms and Bioavailability of Copper to Fish Based on an Adverse Outcome Pathway Analysis. *J. Environ. Sci.* **2023**, *127*, 495–507. [CrossRef] [PubMed]
45. Majda, D.; Makowski, W.; Mańko, M.; Mlekodaj, K.; Michalik-Zym, A.; Napruszewska, B.D.; Zimowska, M.; Serwicka, E.M. Porosity Characterization of SBA-15 Silicas with Thermoporosimetry of Water and n-Alkanes—The Effect of the Probe Liquid Nature. *Microporous Mesoporous Mater.* **2015**, *201*, 141–150. [CrossRef]
46. Smith, A.L. Infrared Spectra-Structure Correlations for Organosilicon Compounds. *Spectrochim. Acta* **1960**, *16*, 87–105. [CrossRef]
47. Büyükmurat, Y.; Akalin, E.; Özel, A.E.; Akyüz, S. Calculation and Analysis of IR Spectrum of 2-Aminopyridine. *J. Mol. Struct.* **1999**, *482–483*, 579–584. [CrossRef]
48. Arkles, B.; Peterson, W.R.; Anderson, R. *Silicon Compounds: Register and Review*, 3rd ed.; Petrarch Systems Inc.: Bristol, PA, USA, 1984.
49. Ahmed, G.S.; Gilberts, M.; Mainprize, S.; Rogerson, M. FTIR Analysis of Silane Grafted High Density Polyethylene. *Plast. Rubber Compos.* **2009**, *38*, 13–20. [CrossRef]
50. Mazinani, B.; Beitollahi, A.; Masrom, A.K.; Ibrahim, S.; Jamil, F. The Effect of Aging Temperature on the Pores of Mesoporous SBA-15 Silica. *AIP Conf. Proc.* **2012**, *1502*, 272–279. [CrossRef]
51. Majda, D.; Napruszewska, B.D.; Zimowska, M.; Makowski, W. Porosity of SBA-15 after Functionalization of the Surface with Aminosilanes. *Microporous Mesoporous Mater.* **2016**, *234*, 98–106. [CrossRef]
52. Wang, X.; Wang, P.; Dong, Z.; Dong, Z.; Ma, Z.; Jiang, J.; Li, R.; Ma, J. Highly Sensitive Fluorescence Probe Based on Functional SBA-15 for Selective Detection of Hg^{2+}. *Nanoscale Res. Lett.* **2010**, *5*, 1468–1473. [CrossRef] [PubMed]

53. Thommes, M. Physical Adsorption Characterization of Nanoporous Materials. *Chem. Ing. Tech.* **2010**, *82*, 1059–1073. [CrossRef]
54. Walcarius, A.; Mercier, L. Mesoporous Organosilica Adsorbents: Nanoengineered Materials for Removal of Organic and Inorganic Pollutants. *J. Mater. Chem.* **2010**, *20*, 4478–4511. [CrossRef]

Disclaimer/Publisher's Note: The statements, opinions and data contained in all publications are solely those of the individual author(s) and contributor(s) and not of MDPI and/or the editor(s). MDPI and/or the editor(s) disclaim responsibility for any injury to people or property resulting from any ideas, methods, instructions or products referred to in the content.